

# **New Particle Formation in Anthropogenic Plumes Advecting from Asia Observed During TRACE-P**

R. J. Weber<sup>1</sup>, S. Lee<sup>1</sup>, G. Chen<sup>2</sup>, B. Wang<sup>1</sup>, V. Kapustin<sup>3</sup>, K. Moore<sup>3</sup>, A. D. Clarke<sup>3</sup>, L.  
Mauldin<sup>4</sup>, E. Kosciuch<sup>4</sup>, C. Cantrell<sup>4</sup>, F. Eisele<sup>1,4</sup>, D. C. Thornton<sup>5</sup>, A. R. Bandy<sup>5</sup>, G. W.  
Sachse<sup>2</sup>, H. E. Fuelberg<sup>6</sup>

<sup>1</sup>School of Earth and Atmospheric Sciences, Georgia Institute of Technology, Atlanta,  
GA

<sup>2</sup>NASA Langley Research Center, Hampton, VA

<sup>3</sup>Department of Oceanography, University of Hawaii at Manoa, Honolulu HI

<sup>4</sup>National Center For Atmospheric Research, Boulder CO

<sup>5</sup>Department of Chemistry, Drexel University, Philadelphia, PA

<sup>6</sup>Department of Meteorology, Florida State University, Tallahassee, FL

## ABSTRACT

The characteristics and sources of what are believed to be newly formed 3-4 nm particles in anthropogenic plumes advecting from Asian are reported. Airborne measurements were made from March to April 2001 as part of the NASA TRACE-P experiment at latitudes ranging from North of the Philippines to Northern Japan (20 to 45°N). In the more polluted plumes, high concentrations of 3 to 4 nm diameter particles ( $>100\text{cm}^{-3}$ ) were observed both within and along the upper outer edges of plumes that were identified by enhanced carbon monoxide and fine particulate sulfate concentrations. The results from two research flights are investigated in detail. 3-4 nm particle concentrations are generally correlated with gas phase sulfuric acid and found in regions where the surface area was lower relative to the immediate surrounding. Sulfuric acid and surface area concentrations in the most polluted plume reached  $6 \times 10^7\text{ cm}^{-3}$  and  $750\text{ }\mu\text{m}^2\text{ cm}^{-3}$ , respectively, in regions of particle formation. In contrast to these anthropogenic plumes, few 3-4 nm particles were observed in the clean background, and few were detected within a volcanic plume where the studies highest  $\text{H}_2\text{SO}_4$  concentrations ( $> 10^8\text{ cm}^{-3}$ ) were recorded. Enhanced  $\text{SO}_2$  concentrations in the range of approximately 2 to 7 ppb, in conjunction with other unidentified, possibly co-emitted species, appear to be the driving factor for nucleation.

## 1. INTRODUCTION

Atmospheric aerosols play a role in global climate through their influence on the Earth's radiation balance. The scattering of solar and terrestrial radiation by aerosols depends on the ambient particle number distribution and particle composition, which are influenced by the rate and prevalence of new particle formation. On more regional scales the source of nanometer-sized particles is of scientific interest due to their possible adverse health effects. Several epidemiological studies [Donaldson *et al.*, 1998; Ferin *et al.*, 1990] have found that ultrafine particles less than 50 nm are correlated to adverse pulmonary diseases, and large increases in the number concentration of ultrafine particles due to homogeneous nucleation have been observed in urban areas [Woo *et al.*, 2001].

Due to their possible climate and health effects, many investigations have been conducted into the mechanism of new particle formation, yet the details are still unknown due to a combination of the complexity of the process and current measurement limitations. Adequate theories and thermodynamic data are lacking for multi-component nucleation. The primary measurement limitation is that nucleation produces new particles of approximately 1 nm diameter, however, current measurement techniques can only detect particles down to roughly 3 nm diameter, significantly larger than the newly formed particles. Thus evidence for nucleation is only detected some time following the event, once the newly formed particles have grown to detectable sizes.

Previous work suggests that  $\text{H}_2\text{SO}_4$  often is a nucleation precursor since nucleation events, indicated by unusually high concentrations of 3-4 nm or concentrations of 3-10 nm diameter particles, is correlated with  $\text{H}_2\text{SO}_4$  concentrations. In the past, binary  $\text{H}_2\text{SO}_4$ - $\text{H}_2\text{O}$  homogeneous nucleation has been considered as the most likely

nucleation mechanism. Previous studies in which  $\text{H}_2\text{SO}_4$  and nm-sized particles were measured, however find that observed particle formation rates cannot be explained by classical binary nucleation theory [Birmili *et al.*, 2000; Birmili and Wiedensohler, 2000; Weber *et al.*, 1995, 1996, 1997, 1998a, 1999].

Ternary nucleation [Coffman and Hegg, 1995; Korhonen *et al.*, 1999] has been proposed as a mechanism that may explain the observations. Experiments show that adding  $\text{NH}_3$  to the binary  $\text{H}_2\text{SO}_4$ - $\text{H}_2\text{O}$  system can increase the rate of new particle formation [Ball *et al.*, 1999]. Some workers have found new particle formation where  $\text{NH}_3$  is expected to play a role [Birmili *et al.*, 2000; Weber *et al.*, 1998a]. An ion-mediated nucleation mechanism is also a possible route for particle formation [Yu and Turco, 2001].

Although many studies have focused on nucleation in remote regions, evidence for nucleation under polluted conditions has also been observed. Increased particle concentrations have been detected at the edges of power plant and smelter plumes [Brock *et al.*, 2002; Wilson, 1978; Williams *et al.*, 1981]. In some cases, the newly formed particles are often found at the edges of relatively fresh plumes (<2 hours old) [Brock *et al.* 2002] where photochemical models predict highest hydroxyl radical (OH) concentrations, and enhanced production of  $\text{H}_2\text{SO}_4$  by oxidation of  $\text{SO}_2$ . McMurry *et al.* [2000] observed new particle formation in urban Atlanta Georgia. In this case, evidence for nucleation was based on events when the sub 10-nm size distribution tailed off to higher concentrations as sizes approached the detection limit of 3 nm. They suggested that nucleation in Atlanta may be explained by a collision-controlled nucleation process involving  $\text{H}_2\text{SO}_4$ .

One objective of the National Atmospheric and Space Administration (NASA) Transport and Chemical Evolution over Pacific (TRACE-P) mission was to investigate the mechanisms and conditions of particle production associated with Asian plumes emanating from the densely populated regions of China, Korea, and Japan. This mission provided an opportunity to sample plumes with varying characteristics, including biomass, volcanic, and urban pollution plumes. We find that high concentrations of 3-4 nm particles are only associated with the pollution plumes. This paper describes the conditions where evidence for recent nucleation was observed from two research flights, and briefly investigates the nucleation mechanism by contrasting the various observations.

## 2. INSTRUMENTATION

The intensive measurement component of TRACE-P ran from February through April 2001. The aim of this multi-investigator experiment was to characterize air masses advected from Asia to gain insights into the physical and chemical processing of gases and aerosol particles in Asian plumes. Two NASA aircraft were involved, a DC-8 and P3-B. Each aircraft made 9 flights near the Asian continental regions to characterize Asian outflow. This paper focuses on the P-3B measurements of sulfur dioxide ( $\text{SO}_2$ ), sulfuric acid ( $\text{H}_2\text{SO}_4$ ), and aerosols.

Sulfur dioxide ( $\text{SO}_2$ ) was measured by an atmospheric pressure ionization mass spectrometer (APIMS) [Thornton *et al.*, 2002]. Sulfuric acid and the hydroxyl radical (OH) were measured by chemical ionization mass spectrometer (CIMS) [Eisele *et al.*, 1993, 1994, 1997]. A number of instruments were deployed for measurements of aerosol number concentration. A modified ultrafine condensation particle counter (TSI 3025, St

Paul MN) equipped with pulse height analysis (PHA-UCPC) measured ultrafine condensation particle concentrations at 1 Hz. Referred to as ultrafine condensation nuclei, this all includes particles larger than  $\sim 3$  nm diameter. Pulse height analysis also allows measurements of concentrations of particles between 3 and 10 nm diameter integrated over 30s. The technique provides information on nanoparticle spectra. We have developed approaches to invert measured pulse height distributions to obtain 3 to 10 nm size distributions [Weber *et al.*, 1998b], however, a simpler approach is used in which only the smallest pulses are counted to determine particle concentrations in a narrow diameter range at the instrument's lower size detection limit, (e.g.,  $\sim 3$  to 4 nm). Although only an estimate of the concentration, the technique is highly sensitive and useful when searching for regions of new particle formation.

A limitation with this technique is that by converting to white-light optics necessary for pulse height analysis, [Marty *et al.*, 1996], the optical detection region is not as highly focused as in the commercial TSI 3025 UCPC, which uses a laser diode. This results in a greater time for individual particles to transit the scattering region of the detector, which increases the probability that more than one particle will be in the scattering region at one time. This so-call coincidence will result in an undercounting of particles when concentrations are high. A dilution system was employed to extend the upper concentration range of the instrument. However, at UCN concentrations higher than approximately  $10,000 \text{ cm}^{-3}$ , coincidence becomes significant and the UCN measurements are more uncertain, (on the order of  $\pm 50\%$ ). The UCN and 3-4 nm particle concentrations reported in this paper are converted to standard temperature and pressure (20°C and 1 atmosphere).

Ambient aerosol size distributions of fine and coarse particles were measured with a variety of instruments. Our interest is in the interaction of the gases (e.g.,  $\text{H}_2\text{SO}_4$ ) and newly formed particles with the preexisting aerosol, which requires a measurement of the aerosol number distribution. Measurements of the dry (heated to  $40^\circ\text{C}$ ) distribution of particles between  $0.15$  and  $19\text{ }\mu\text{m}$  was made in the aircraft cabin via a shrouded isokinetic inlet with an Optical Particle Counter (OPC, PMS LAS-X, Boulder, CO). Because the inlet temperature was cycled to investigate changes in the distribution to particle volatility, size distributions were integrated over one minute but often measured only once every 3 minutes. Ambient wet particle size distributions are estimated by assuming accumulation mode particles (diameters less than  $0.6\text{ }\mu\text{m}$  diameter) absorb water as a generic marine aerosol [Swietlicki *et al.*, 2000], and coarse mode particles behave as dust and don't absorb water. The measured surface areas are uncertain for a number of reasons: 1) Inlet and sampling losses of particles with diameters larger than approximately  $3\text{ }\mu\text{m}$ . 2) Losses of semi-volatile material, other than water, on heating the particles to  $40^\circ\text{C}$ . 3) Uncertainties associated with converting the dry distribution to ambient size distributions by calculating the aerosol particle uptake of water.

A wing-mounted Forward Scattering Spectrometer Probe 300 (FSSP;  $0.3 \sim 20\text{ }\mu\text{m}$  diameter) provide particle liquid water content data, which is used to identify spurious UCN data due to sampling artifacts associated with droplet shatter on the aerosol sampling inlet [Weber *et al.*, 1998c]. Evidence of shatter has been removed from the data set for this analysis.

The bulk ionic composition of fine particles was measured continuously and in near real-time with a Particle Into Liquid Sampler, PILS [Orsini and Weber, 2002; Weber *et al.*, 2001b]. The anions; chloride, nitrate, and sulfate, and cations; sodium, ammonium, potassium, magnesium, and calcium were measured at a rate of every 4 minutes.

### 3. THEORY

In the following discussion, a number of factors are calculated to aid in the analysis. This includes the sulfuric relative acidity, the loss of H<sub>2</sub>SO<sub>4</sub> and newly formed 1.5-nm-diameter particles by preexisting particle scavenging, and the production rate of H<sub>2</sub>SO<sub>4</sub> and its predicted steady state concentration.

**Sulfuric Relative Acidity:** Classical nucleation theory predicts that nucleation rates depend on the degree of vapor saturation (e.g., Wilemski, 1984), and a measure of H<sub>2</sub>SO<sub>4</sub> vapor saturation is the sulfuric relative acidity (RA). RA is calculated from the measured H<sub>2</sub>SO<sub>4</sub> concentration, (this includes all monoacid hydrates), divided by the saturation concentration of pure acid over a flat surface, given as the partial pressure in atmospheres ( $p$ ) by Ayers *et al.* [Ayers *et al.*, 1980] as;

$$p = \exp(-10156/T + 16.259) \quad (1)$$

where  $T$  is the absolute temperature.

**Scavenging of H<sub>2</sub>SO<sub>4</sub> and 1.5 nm diameter particle:** The loss rate of H<sub>2</sub>SO<sub>4</sub> and 1.5-nm particles by absorption onto the preexisting aerosol particles is calculated using the method of Fuchs-Sutugin [1970] as we have done in other studies [Eisele and Tanner, 1993; Jefferson *et al.*, 1998; Weber *et al.*, 2001a; Weber *et al.*, 1997] For the calculation of H<sub>2</sub>SO<sub>4</sub> scavenging, an accommodation coefficient of 0.72 is assumed [Jefferson *et al.*,

1997], the hydrated  $\text{H}_2\text{SO}_4$  molecule diffusivity of  $0.08 \text{ cm}^2 \text{ s}^{-1}$  [Roedel, 1979] and effect of ambient temperature and RH on monomer mass is estimated from bulk properties [Gmitro and Vermeulen, 1963] and used to calculate the monomer average thermal speed.

Scavenging losses of newly formed particles are estimated by calculating the loss of a 1.5 nm diameter particle, as a surrogate for particles between 1 and 3 nm diameter, using the same method as that for  $\text{H}_2\text{SO}_4$ . In this case we assume an accommodation coefficient of 1, and the 1.5 nm-particle thermal speed is calculated as a function of temperature and a constant relative humidity of 50%, and a calculated diffusivity. In both calculations, the inverse of the Fuchs Sutugin first order loss rate constant ( $k'$ , units  $1/\text{s}$ ) is the characteristic (*e-folding*) scavenging time.

***$\text{H}_2\text{SO}_4$  production rates and calculated steady state concentrations.*** The rate at which  $\text{H}_2\text{SO}_4$  vapor is produced is calculated by:

$$R = k [\text{OH}] [\text{SO}_2] \quad (2)$$

where the rate constant,  $k$  depends on ambient temperature and pressure and ranges from  $7$  to  $9 \times 10^{-13} \text{ cm}^3 \text{ s}^{-1}$  [DeMore *et al.*, 1992]. Since in these plumes the  $\text{H}_2\text{SO}_4$  scavenging rates ( $k'$ ) are high,  $\text{H}_2\text{SO}_4$  is likely in a steady state balance between production and loss. This is likely a good approximation since typical  $\text{H}_2\text{SO}_4$  lifetimes are in the range of less than a minute to 4 minutes (see Table 1). The calculated steady state acid concentration is then:

$$[\text{H}_2\text{SO}_4]_c = R/k'. \quad (3)$$

In the following analysis the continuity between  $\text{SO}_2$ ,  $\text{H}_2\text{SO}_4$ , and the preexisting ambient aerosol distribution is assessed by comparing measured  $\text{H}_2\text{SO}_4$  concentrations to  $[\text{H}_2\text{SO}_4]_c$ .

#### 4. OBSERVATIONS

TRACE-P was conducted from March to mid-April from two bases of operation. Flights were first made from Hong Kong, Peoples Republic of China, from March 5 to 16, 2001. The aircraft was then based out of Yokota Air Force Base near Tokyo, Japan, March 17 to April 3, 2001. The geographical region investigated is shown in Figure 1. A variety of plumes were sampled during the study and are identified by the gaseous and fine particle chemical components. High CO, SO<sub>2</sub>, and fine particle sulfate (SO<sub>4</sub><sup>2-</sup>) concentrations identify the anthropogenic plumes. CO and SO<sub>2</sub> indicate combustion sources, and SO<sub>4</sub><sup>2-</sup> is from gas-to-particle conversion of anthropogenic SO<sub>2</sub> and provides a measure of the aerosol loading, assuming that the biogenic SO<sub>2</sub> sources in this region are small in comparison to the anthropogenic emissions. There is also a volcanic SO<sub>2</sub> source from Miyake-Jima, Japan, which is identified by high SO<sub>2</sub> concentrations and a lack of CO. Fine particle potassium and CO, along with other species, identified biomass burning emissions. The role of biomass burning on fine particle composition is discussed in Ma et al [2002].

Several flights with plumes of unique characteristics, and the regions with high 3-4 nm particle concentration, are also highlighted in Figure 1. Frequent encounters with well-defined plumes were made near the Asian continental areas during the TRACE-P experiment. For example, in flight 10 a relatively pure biomass plume was identified, a volcanic plume on flight 17, and encounters with large anthropogenic plumes during flights 14 and 19, also identified in the figure.

No 3-4 nm particles were observed in the biomass plume (flight 10) which contained low SO<sub>2</sub> concentrations measured at ~200 pptv, and correspondingly low

$\text{H}_2\text{SO}_4$  concentrations at less than  $2 \times 10^6 \text{ cm}^{-3}$ . Apparently, no organic species nucleated to form new particles in the biomass plume in the region sampled. The volcanic plume (flight 17) had high  $\text{SO}_2$  concentrations, but contained only low 3-4 nm particle concentrations ( $<10 \text{ cm}^{-3}$ , see Table 1 (F)) suggesting that there was little particle production in this plume when our measurements were made. In contrast, high 3-4 nm particle concentrations ( $> 100 \text{ cm}^{-3}$ ) were often observed associated with anthropogenic plumes. Of these, the most extensive regions of new particle formation observed during TRACE-P were recorded on two flights, 14 and 19. 3-4 nm particle production associated with these plumes is investigated in detail in the following sections.

***Case Study 1: Sea of Japan, flight 19.*** Figure 2 shows the flight path over the Sea of Japan and identifies the pollution plumes. Florida State University's Kinematic Trajectory Model using the three wind components derived from the European Center for Medium-Range Weather Forecasts (ECMWF) calculated 5-day back-trajectories. For more detail see, *Fuelberg et al.*, [2000] and *Maloney et al.*, [2001]. The back-trajectory analysis in Figure 2 illustrates that the air masses sampled had passed over the highly populated and industrial regions of western China and may have been impacted by the cities of Beijing, Tianjin, or Qingdao. The plumes then traveled across the Yellow Sea and South Korea below 1 km altitude prior to entering the Sea of Japan. These air masses likely acquired pollutants from urban centers in both China and Korea. Here we focus on the flight conducted in the vicinity of  $38^\circ\text{N}$  latitude and  $135^\circ\text{E}$  longitude between roughly 1100 ~ 1330 local sun time.

The time series of various measurements near and within the plume are shown in Figure 3. The altitude shows a number of soundings and horizontal legs during this

period, the longest leg below 1km asl. Based on CO and  $\text{SO}_4^{2-}$  concentrations, in Figure 3b, and comparing to the altitude, a large anthropogenic plume was intercepted and constrained to altitudes below approximately 1.5 km asl. Although the two surface level measurements where the plume is detected are actually made in different regions in the Sea of Japan (see Figure 2), the back-trajectory analysis indicates that both likely had a similar origin, suggesting it may be a single large plume. Figure 3c shows that the  $\text{H}_2\text{SO}_4$  and  $\text{SO}_2$  concentrations also increased with the CO and  $\text{SO}_4^{2-}$  concentrations, and that  $\text{H}_2\text{SO}_4$  and  $\text{SO}_2$  are fairly well correlated.

UCN (all particles larger than 3 nm) in Figure 3d are also enhanced in the plumes and generally track the CO concentration defining the plume boundaries. 3-4 nm particles are near zero at the higher altitudes above the plume and also within the plume during the lowest altitude leg near the ocean surface. However, high concentrations are detected in distinct regions, highlighted in Figure 3 by the shaded vertical bands. Comparison of these 3-4 nm particle regions with altitude shows that over this wide geographical region where the aircraft sampled in and out of the plume, there is a well defined altitude range between roughly 1 and 2.7 km asl where 3-4 nm particles were always detected. The crosshatched box in Figure 3a identifies the altitude of this region.

High 3-4 nm and UCN particles (shaded areas in Figure 3) appear to be associated with the high  $\text{H}_2\text{SO}_4$  concentrations and suggests that  $\text{H}_2\text{SO}_4$  may have participated in new particle production in these regions. However, note that there are regions within the plume near the ocean surface where concentrations of  $\text{H}_2\text{SO}_4$  are similar to the 3-4 nm particle regions, but where 3-4 nm particle concentrations are very low. These regions have much higher aerosol surface area concentrations, whereas the 3-4 nm particle

regions are found where surface areas are lowest. On average the characteristic lifetime of a 1.5 nm particle ( $1/k'$ ) within the plumes is about 6 minutes, compared to 14 minutes in the 3-4-nm regions. These, and various other measurements in the 3-4 nm particle regions, and within the plume, are summarized in Table 1 sections A and B.

The unique 3-4 nm particle regions associated with this plume are investigated in more detail by plotting the vertical profiles. Means from the four separate soundings, and the “error bar”, indicating maximum and minimum measurements, are shown in Figure 4. The shaded region in each graph in Figure 4, spanning 1.0 to 2.7 km asl, is the region of enhanced 3-4 nm particle concentrations. The temperature profile shows a weak inversion at about 1.0 km asl. The band of 3-4 nm particles is found mainly above the inversion in a dryer layer, as seen by the relative humidity profile. CO concentrations, which identifies the location of the plume, begin to decrease above 1 km asl as the plume is diluted into the cleaner air above. This is the region where 3-4 nm particle concentrations start to increase with altitude.

SO<sub>2</sub> levels tend to follow the CO, with the exception that they begin to decrease at a slightly higher altitude of 1.3 km asl, overlapping the lower altitude region of 3-4 nm particles. H<sub>2</sub>SO<sub>4</sub> has a similar vertical trend; it generally follows both CO and SO<sub>2</sub>, but on average does not begin to decrease until higher altitudes. Notice that highest H<sub>2</sub>SO<sub>4</sub> concentrations are found right at the inversion, on the upper edge of the plume. Aerosol surface areas are highest in the plume, than drop above the plume, similar to CO.

The fine particle ionic composition of the plume is shown in Figure 5. In this case concentrations are given as mass at 20°C and 1 atmosphere pressure. The measured cations and anions are nearly balanced. The molar ratio of [cations-anions] to the sum of

all ions is less than 1%. Furthermore, sulfate and nitrate are nearly balanced by ammonium, suggesting that the main ionic components of the fine aerosol particles are ammonium sulfate and ammonium nitrate salts.

***Case Study 2, Yellow Sea Plume, Flight 14.*** In contrast to the Sea of Japan plume, a plume comprised of some of the highest CO, SO<sub>2</sub> (with the exception of the volcanic plume-flight 17) and fine particle sulfate and nitrate of the entire TRACE-P mission was intercepted at the surface in the Yellow Sea at 35 °N Latitude and 124.5 °E Longitude (See Figure 6). Back trajectories indicate that the surface level air masses were arriving directly from the west, a path similar to the plume intercepted in the Sea of Japan, detailed in Case Study 1 above, and which may have picked up pollution from the large cities such as Tianjin, and Qingdao, China. In this case, however, the plume was likely intercepted closer to its main source. Ratios of  $\text{SO}_4^{2-}/(\text{SO}_4^{2-} + \text{SO}_2)$ , which can provide a measure of plume age, are smaller in this plume than those of Flight 14 suggesting the plume is fresher (Ft 14 ratio is 0.42 and Ft 19, 0.51).

This plume was intercepted on the lowest altitude leg, below 1 km asl, at roughly 1200~1300 local sun time. Time series plots, similar to those for the Sea of Japan plume of Case 1, are shown in Figure 7. CO and SO<sub>4</sub><sup>2-</sup> concentrations identify the plume, which in this case are about double those of the Sea of Japan plume in Figure 3. SO<sub>2</sub> and H<sub>2</sub>SO<sub>4</sub> track almost precisely. (This is likely a result of the very short H<sub>2</sub>SO<sub>4</sub> lifetime due to rapid scavenging and the high acid production rates. This is discussed in the following section). Both SO<sub>2</sub> and H<sub>2</sub>SO<sub>4</sub> have peak concentrations that are the highest for the complete TRACE-P mission, except those in the volcanic plumes (Miyake-Jima, Japan)

of flight 17. Note that  $\text{H}_2\text{SO}_4$  data is only available during the first half of the plume measurement.

Concentrations of UCN and 3-4 nm particles, shown in Figure 7d, also roughly track the  $\text{CO}$ ,  $\text{SO}_4^{2-}$ ,  $\text{SO}_2$ , and  $\text{H}_2\text{SO}_4$ . The altitude ranges where 3-4 nm particles are detected, are identified by shading in Figure 7a and vary in altitude from the surface up to 1.8 km asl, and up to 3.4 km asl. In this plume, 3-4 nm particles are observed both in regions slightly above the plume and completely throughout the plume, with the exception of the plume center where RH is greater than 85%. Again, nanoparticle concentrations tend to be highest in regions of higher  $\text{SO}_2$  and  $\text{H}_2\text{SO}_4$ .

Aerosol surface area concentrations increase toward the center of the plume where the relative humidity is over 85%. In this central region,  $\text{CO}$  and  $\text{SO}_4^{2-}$  concentrations were slightly lower, and  $\text{SO}_2$  and  $\text{H}_2\text{SO}_4$  were significantly reduced. No 3-4 nm particles were found in this region. The data from the two 3-4nm bands are summarized in Table 1 section (C), and the region of no 3-4nm particles is summarized in section (D).

Vertical profiles are plotted in Figure 8. In this case two soundings were made, and data from both are plotted. Temperature profiles show that the boundary layer was very shallow with an inversion at 30 m asl. Based on  $\text{CO}$  concentrations, the plume extended considerably above the inversion to about 1.8 to 2 km asl.  $\text{SO}_2$  and  $\text{H}_2\text{SO}_4$  concentrations are highly correlated, however, unlike the Sea of Japan plume, in this case the 3-4 nm particles are not as well correlated with  $\text{H}_2\text{SO}_4$ . The figure shows that 3-4nm particles are found throughout the plume and into the dilution region above it.

The plume's fine particle ionic composition is shown in Figure 9. Note the much higher concentrations compared to Case 1, in Figure 6. This plume is unusual in that nitrate concentrations exceed sulfate. An ion balance suggest that most of the sulfate and nitrate is associated with ammonium (e.g.,  $(\text{NH}_4)_2\text{SO}_4$  and  $\text{NH}_4\text{NO}_3$ ). Another interesting feature of this plume is the potassium concentrations ( $\text{K}^+$ ), which are the highest  $\text{K}^+$  concentrations recorded during this mission and are thought to be associated with biomass burning emissions [Ma *et al.*, 2002].

Not all plumes investigated in this study showed evidence of nanoparticle production. During flight 19 in the Sea of Japan, two other anthropogenic plumes were intercepted on horizontal legs at less than 1 km asl. In this case,  $\text{SO}_2$  concentrations are much lower, near  $\sim 0.2$  ppbv, as are both  $\text{H}_2\text{SO}_4$ , with an average concentration of  $3 \times 10^6 \text{ cm}^{-3}$ , and 3-4 nm particle concentrations, which averaged less than  $1 \text{ cm}^{-3}$ . These case studies, and the apparent lack of particle production in plumes of low  $\text{H}_2\text{SO}_4$  concentrations, point to the role of  $\text{H}_2\text{SO}_4$  in particle production, and indirectly to the importance of  $\text{SO}_2$  concentrations.

## 5. DISCUSSION

Concentrations of newly formed nanoparticles depend on the homogeneous nucleation rate and the rate at which they are lost and dispersed. Because the time scales for nanoparticle scavenging near and within these polluted plumes are very small, on the order of 5 to 15 minutes ( $1/k'$ , Table 1), particle loss by dry deposition, dispersion, and dilution are in comparison of minor importance. It follows then that highest 3-4 nm concentrations would be expected in regions of highest nucleation rates (i.e., precursor concentrations, such as  $\text{H}_2\text{SO}_4$ ) and lowest scavenging rates (i.e., lowest 3-4 nm mass

transfer rate constants,  $k'$ , or roughly aerosol surface area concentrations). For a given plume, this is generally consistent with the observations. In each plume the 3-4 nm particles tend to be associated with high acid concentrations and found where surface areas are low with respect to the immediate surroundings. This is most clearly seen in the Case 1 Sea of Japan plume in Figure 3 where 3-4 nm particles are found in the regions of highest  $\text{H}_2\text{SO}_4$  concentrations where the area is low, but not in the plume at similar acid level where the surface area is high.

Another consequence of the high scavenging rates of  $\text{H}_2\text{SO}_4$  and 3-4 nm particles is that their concentrations will respond rapidly to changes in ambient conditions. Thus the conditions where 3-4 nm particles are observed are likely very close to those in which homogeneous nucleation occurred. It is also noted that the high scavenging rates of newly formed particles imply that particle growth rates must also be too high to compensate, or else few newly formed particles would be detected.

Contrasting the nucleation regions of the two pollution plumes also provides some insights into conditions under which particle production can occur. There are significant differences in the regions of homogeneous nucleation, for the two plumes discussed above. For example, despite higher  $\text{H}_2\text{SO}_4$  mass transfer rates to the preexisting particles ( $\text{H}_2\text{SO}_4 k'$ ) in the Yellow Sea plume,  $\text{H}_2\text{SO}_4$  concentrations were on average three times high in the nanoparticle regions (see Figures 3 and 7, and Table 1). This implies that the production rate of  $\text{H}_2\text{SO}_4$  must have been considerably higher in this plume to offset its loss by particle scavenging and to maintain the higher acid concentrations. The average  $\text{H}_2\text{SO}_4$  production rates in the more polluted Yellow Sea plume (Flight 14, Case 2) are  $1 \times 10^6 \text{ cm}^{-3} \text{ s}^{-1}$ , about an order of magnitude higher than those in the Sea of Japan plume

(Flight 19, Case 1) which on average are  $2 \times 10^5 \text{ cm}^{-3} \text{ s}^{-1}$ . A comparison shows that the high acid production rate is due to higher concentrations of both  $\text{SO}_2$  and OH. However, larger  $\text{SO}_2$  appears to be the more dominant factor; OH concentrations in the Yellow Sea plume are a factor of 2 larger and  $\text{SO}_2$  a factor of 4 larger.

The interaction between  $\text{H}_2\text{SO}_4$  production and loss by scavenging can be used to predict ambient  $\text{H}_2\text{SO}_4$  concentrations. The consistency between the measurements of  $\text{SO}_2$ ,  $\text{H}_2\text{SO}_4$ , and the preexisting aerosol is now investigated by comparing observed and calculated steady state  $\text{H}_2\text{SO}_4$  concentrations.

***Continuity between  $\text{SO}_2$ ,  $\text{H}_2\text{SO}_4$ , and the preexisting particles.*** Because  $\text{SO}_2$ , through the production of  $\text{H}_2\text{SO}_4$ , and the preexisting particles appear to play major roles in determining the production of nanoparticles near and within these plumes, the continuity between these measurements is investigated. Ambient  $\text{H}_2\text{SO}_4$  concentrations are calculated by Eq (3), which assumes steady state between the acid source via OH- $\text{SO}_2$  reaction, Eq (2), and sink by pre-existing particle scavenging. A similar analysis for measurements in clean remote regions show that calculated and measured concentrations of  $\text{H}_2\text{SO}_4$  are in good agreement [Eisele and Tanner, 1993; Weber et al., 1997].

The results of this calculation for the measurements near and within the plumes shown in Figures 3 and 7, are summarized in Figure 10. These scatter plots indicate that the measured and calculated  $\text{H}_2\text{SO}_4$  concentrations are in fairly close agreement for the more polluted Yellow Sea plume of Flight 14, Case 2, where the slope is within 10%. For the Sea of Japan plume of Flight 19, Case 1, the calculated  $\text{H}_2\text{SO}_4$  is approximately twice the observed. In both cases the correlation is fairly high indicating the trends in the measured  $\text{H}_2\text{SO}_4$  are captured by the variations in  $\text{SO}_2$ , OH, and aerosol distribution.

The cause for the higher predicted concentration for the Sea of Japan plume is not known and difficult to explain given the much better agreement for the Yellow Sea plume. It could be that the measured  $\text{SO}_2$  or OH concentrations are too high, the measured  $\text{H}_2\text{SO}_4$  is too low, or that the measured preexisting particle distribution is too low. The aerosol distribution used to calculate the Fuch-Sutugin mass transfer rates is likely the most uncertain. The mass transfer rates may be too low for a number of reasons: One, the complete distribution is not measured. However, Figure 11 shows example surface area distributions for measurements within the two plumes. The plot shows that most of the  $\text{H}_2\text{SO}_4$  uptake is in the accumulation mode by particles between 0.1 and 1  $\mu\text{m}$  diameter, and that most of the distribution is apparently measured by the optical particle counter. Fuchs-Sutugin mass uptake rate constants in which particles smaller than 0.1  $\mu\text{m}$  are included (measured with a differential mobility analyzer) are increased by less than 10% so the role of smaller particles is minor and can be ignored. A second uncertainty associated with the preexisting particle distribution is that the calculation of the ambient wet distribution from measured dry distributions under estimates the amount of water uptake by the particles. This is also an unlikely explanation since the bulk particle ionic composition for particles less than roughly 1.3  $\mu\text{m}$  diameter shown in Figures 5 and 9 are very similar for the two plumes. In both cases the ionic component of the aerosol particles are ammonium nitrate and sulfate salts. Thus unless the water uptake of the unmeasured organic component was vastly different between the plumes, the modeled water uptake should be similar in both cases. In the current analysis the coarse particles are not assumed to take up water. Repeating the calculations assuming coarse sea-salt particles does significantly change the predicted  $\text{H}_2\text{SO}_4$  concentrations. Although

we lack an explanation for the discrepancy, the trends in the  $\text{SO}_2$ ,  $\text{H}_2\text{SO}_4$ , and preexisting particles are consistent, however the combined uncertainty in these measurements may be on the order of 200%.

Finally, this analysis shows that  $\text{H}_2\text{SO}_4$  and preexisting aerosol particle concentrations are coupled through scavenging. As the plume ages  $\text{H}_2\text{SO}_4$  concentrations should drop and at some point new particle formation should cease, due to the combined effect of reductions in  $\text{SO}_2$  as it is consumed, reducing  $\text{H}_2\text{SO}_4$  production rates, and an increase in the rate of  $\text{H}_2\text{SO}_4$  scavenged as gas-to-particle conversion over time increases the aerosol surface area. Clearly the plumes we have investigated have not reach that point. An idea on how long it takes for a typical plume to reach that point would be of interest from both a health effects and a radiative forcing standpoint. Model predictions could provide insight into the time scales for quenching nucleation in these types of plumes.

***Nucleation Mechanism.*** The plumes discussed in this paper contain the highest 3-4 nm particle concentrations recorded during TRACE-P. The mechanism that led to particle production remains unclear, however, the observations are not well explained by some theories. The data suggest  $\text{H}_2\text{SO}_4$  plays a role, and most nucleation mechanism assume the same. Predictions for binary  $\text{H}_2\text{SO}_4$ - $\text{H}_2\text{O}$  nucleation rates using current models [Kulmala *et al.*, 1998] suggest that  $\text{H}_2\text{SO}_4$  concentrations of roughly two orders of magnitude higher than those observed are necessary for particle production in these regions.

The inability of binary nucleation to predict the observations in the anthropogenic plumes is further demonstrated by comparing the anthropogenic plumes to the volcanic

plume intercepted on flight 17, emanating from Miyake-Jima, on the Island of Izu, Japan (34.08 °N, 139.53 °E). This plume is identified by high SO<sub>2</sub> (over 10 ppbv) and very low CO concentrations (233 ppbv). The 5-day back trajectories also confirm emissions from Miyake-Jima. Data from this plume are summarized in Table 1 section (F).

A comparison between the concentrations of newly formed 3-4 particles and H<sub>2</sub>SO<sub>4</sub> concentrations in the nucleation regions of the two pollution plume Case Studies, to those in the volcanic plume is shown in Figure 12. In the anthropogenic plumes, higher nanoparticle concentrations are associated with higher H<sub>2</sub>SO<sub>4</sub> concentrations, but not for the volcanic plume. Binary nucleation rates depend mainly on the relative humidity and H<sub>2</sub>SO<sub>4</sub> relative acidity. Comparisons based on data from Table 1 show that the conditions most optimal for binary nucleation are found in the volcanic plume. The relative humidity is higher than that in the 3-4 nm regions of flight 14 and 19 plumes, and the relative acidity is over two times higher. The measurement of few 3-4 nm particles in the volcanic plume compared to the anthropogenic plumes is further evidence that other gaseous species are required for particle production, and that binary H<sub>2</sub>SO<sub>4</sub>-H<sub>2</sub>O nucleation can likely be excluded as the mechanism.

Modeling [*Kerminen et al.*, 2001; *Korhonen et al.*, 1999] and experimental results [*Ball et al.*, 1999] show nucleation is possible at H<sub>2</sub>SO<sub>4</sub> concentrations on the order of 10<sup>7</sup> cm<sup>-3</sup>, if NH<sub>3</sub> is greater than 20 pptv (25°C). These acid concentrations are similar to our observations. Although NH<sub>3</sub> was not measured, the fine particle ionic composition data suggest significant levels of NH<sub>3</sub> were likely associated with the plumes, based on particulate ammonium (NH<sub>4</sub><sup>+</sup>) as an indirect indicator for the availability of NH<sub>3</sub>. Figures 5 and 9 show that NH<sub>4</sub><sup>+</sup> was the main neutralizing agent of the acid aerosol species, with

concentrations much higher than the other aerosol cations (i.e.,  $\text{Na}^+$ ,  $\text{K}^+$ ,  $\text{Mg}^{2+}$  and  $\text{Ca}^{2+}$ ), and a significant amount of the ammonium was likely in the form of ammonium nitrate ( $\text{NH}_3\text{NO}_3$ ). Since  $\text{NH}_3\text{NO}_3$  will only form once all sulfate aerosol is neutralized [Seinfeld and Pandis, 1998], the presence of  $\text{NH}_3\text{NO}_3$  suggests available  $\text{NH}_3$ . In the volcanic plume where no 3-4nm particles were observed there was insufficient  $\text{NH}_4^+$  to neutralize the  $\text{SO}_4^{2-}$ .  $\text{NH}_4^+/\text{SO}_4^{2-}$  molar ratios in the volcanic plumes were typically less than 1. Thus the fine particle data supports the view that the anthropogenic plumes were not depleted of  $\text{NH}_3$  and the volcanic plume was. Note that nucleation mechanisms other than  $\text{H}_2\text{SO}_4$ - $\text{NH}_3$ - $\text{H}_2\text{O}$  are possible, however, the data do suggest that particle production in these plumes was limited by  $\text{H}_2\text{SO}_4$  concentrations and that other species associated with the plumes also played a role.

## 6. SUMMARY

Measurements near the sources of Asian outflow from populated regions provided an opportunity to study new particle formation in anthropogenic plumes. Based on simultaneous measurements of various parameters,  $\text{H}_2\text{SO}_4$  and the aerosol surface area concentrations appear to have the largest influence on 3-4 nm particle concentrations. The characteristic lifetime of these particles due to scavenging by the larger particles is estimated to be less than approximately 15 minutes. The particles were thus likely to have been only recently produced in situ by homogeneous nucleation.

Two different anthropogenic plumes are investigated in detail. In both, distinct increases in 3-4nm particle concentrations are found in regions of high  $\text{H}_2\text{SO}_4$  and surface areas that are low relative to immediate surroundings, often corresponding to dryer regions. These regions were observed near the edges of the plumes where dilution had

occurred, and in one case within the plume itself. For a plume observed in the Sea of Japan, nucleation was only observed in the near-plume field where dilution appears to play a key role in producing conditions for nucleation. For this plume,  $\text{SO}_2$  concentration of  $\sim 2$  ppbv, and surface areas of  $\sim 20 \text{ } \mu\text{m}^2\text{cm}^{-3}$  resulted in  $\text{H}_2\text{SO}_4$  concentrations of  $\sim 2 \times 10^7 \text{ cm}^{-3}$  ( $2^\circ\text{C}$ ), and nucleation. No nucleation was observed within this plume despite similar  $\text{H}_2\text{SO}_4$  concentrations but where particle surface areas were much higher, at  $170 \text{ } \mu\text{m}^2\text{cm}^{-3}$ . In contrast, nucleation was observed both near and within the most heavily polluted plume encountered on the NASA P3 aircraft during TRACE P. In this case particle production was observed in a region where  $\text{SO}_2$  concentrations were roughly 8 ppbv, particle surface areas of  $\sim 750 \text{ } \mu\text{m}^2\text{cm}^{-3}$ , and  $\text{H}_2\text{SO}_4$  concentrations of  $1 \text{ to } 6 \times 10^7 \text{ cm}^{-3}$  ( $10^\circ\text{C}$ ). Nearby within the center of the plume, no nucleation was observed where  $\text{SO}_2$  levels were 3 pptv and surface areas were  $1600 \text{ } \mu\text{m}^2\text{cm}^{-3}$ . These results show that even highly polluted plumes with high aerosol surface area concentrations can support regions of new particle formation if  $\text{SO}_2$  concentrations are sufficient.

Contrasting these plumes to a volcanic plume of higher  $\text{H}_2\text{SO}_4$  concentrations but with little 3-4 nm particles shows that nucleation was not via a binary  $\text{H}_2\text{SO}_4$  and  $\text{H}_2\text{O}$  mechanism. Measurements of the fine particle ionic composition indicate that both plumes have ammonium to sulfate molar ratios from 3 to 5 in the nucleation regions apparently due to the presence of ammonium nitrate, compared to molar ratios less than 1 in the volcanic plume. These results are consistent with the presence of excess ammonia in the nucleating plumes suggesting the possible participation of ammonia through a ternary  $\text{H}_2\text{SO}_4\text{-NH}_3\text{-H}_2\text{O}$  mechanism.

## REFERENCE

- Ayers, G.P., R.W. Gillett, and J.L. Gras, On the vapor pressure of sulfuric acid, *Geophys. Res. Lett.*, 7,433-7,436, 1980.
- Ball, S.M., D.R. Hanson, F.L. Eisele, P.H. McMurry, Laboratory studies of particle nucleation: Initial results for H<sub>2</sub>SO<sub>4</sub>, H<sub>2</sub>O, and NH<sub>3</sub> vapors, *J. Geophys. Res.*, 104, 23,709-23,718, 1999.
- Birmili, W., A. Wiedensohler, C. Plass-Dulmer, H. Berresheim, Evolution of newly formed aerosol particles in the continental boundary layer: A case study including OH and H<sub>2</sub>SO<sub>4</sub> measurements, *Geophys. Res. Lett.*, 27, 2205-2208, 2000.
- Birmili, W. and A. Wiedensohler, New particle formation in the continental boundary layer: Meteorological and gas phase parameter influence, *Geophys. Res. Lett.*, 27, 3325-3328, 2000.
- Brock, C.A., R.A. Washenfelder, M. Trainer, T.B. Ryerson, J.C. Wilson, J. M. Reeves, L.G. Huey, J.S. Holloway, D.D. Parrish, G. Hubler, F.C. Fehsenfeld, Particle growth in the plumes of coal-fired power plant, *J. Geophys. Res.*, 107, AAC 9-1 – AAC 9-11, 2002.
- Coffman, D.J., and D.A. Hegg, A preliminary study of the effect of ammonia on particle nucleation in the marine boundary layer, *J. Geophys. Res.*, 100, 7147-7160, 1995.
- DeMore, W.B., S.P. Sander, D.M. Golden, R.F. Hampson, M.J. Kurylo, C.J. Howard, A.R. Ravishankara, C.E. Kolb, M.J. Molina, Chemical kinetics and photochemical data for use in stratospheric modeling, evaluation no. 10., *Jet Propulsion Laboratory*, 92-20, 1992.

- Donaldson, K., X.Y. Li, W. MacNee, Ultrafine (nanometer) particle mediated lung injury, *J. Aerosol Sci.*, 29, 553-560, 1998.
- Eisele, F.L., and D.J. Tanner, Measurements of the gas phase concentrations of  $\text{H}_2\text{SO}_4$  and Methane Sulfonic acid and estimates of  $\text{H}_2\text{SO}_4$  production and loss in the atmosphere, *J. Geophys. Res.*, 98, 9001-9010, 1993.
- Eisele, F.L., G.H. Mount, F.C. Fehsenfeld, J. Harder, E. Marovich, J. Roberts, D.J. Tanner, M. Trainer, An intercomparison of tropospheric OH and ancillary trace gas measurements at Fritz Peak Observatory, Colorado, *J. Geophys. Res.*, 99, 18,605, 1994.
- Eisele, F.L., R.L. Mauldin III, D.J. Tanner, J.R. Fox, T. Mouch, T. Scully, An inlet sampling duct for airborne OH and sulfuric acid measurements, *J. Geophys. Res.*, 102, 27,993-28,002, 1997.
- Ferin, J., Oberdorster, D.P. Penney, S.C. Soderholm, R. Gelein, H. C. Piper, Increased pulmonary toxicity of ultrafine particles? I. Particle clearance, translocation, morphology, *J. Aerosol Sci.*, 21, 381-384, 1990.
- Fuchs, N.A., and A.G. Sutugin, Highly Dispersed Aerosols, *Butterworth-Heinemann, Newton, Mass.*, 47-60, 1970.
- Fuelberg, H.E., J.R. Hannan, P.F.J. Van Velthoven, E.V. Browell, G. Bieberbach Jr., R.D. Knabb, G.L. Gregory, K.E. Pichering, and H.B. Selkirk, A meteorological overview of the SONEX period, *J. Geophys. Res.*, 105, 3633-3651, 2000.
- Gmitro, J., and T. Vermeulen, Vapor-liquid equilibrium for aqueous sulfuric acid, *UCRL-10886, LRL Rep. TID-4500 Univ. of Calif. Berkeley*, 81, 1963.

- Jaecker-Voiral, A., and Mirable, P., Heteromolecular nucleation in the sulfuric acid-water system, *Atmos. Environ.*, 23, 2053-2057, 1989.
- Jefferson, A., F.L. Eisele, P.J. Ziemann, J.J. Marti, R.J. Weber, and P.H. McMurry, Measurements of the H<sub>2</sub>SO<sub>4</sub> mass accommodation coefficient onto polydisperse aerosol, *J. Geophys. Res.*, 102, 19021-19028, 1997.
- Jefferson, A., D.J. Tanner, F.L. Eisele, and H. Berresheim, Sources and sinks of H<sub>2</sub>SO<sub>4</sub> in the remote Antarctic marine boundary layer, *J. Geophys. Res.*, 103, 1639-1645, 1998.
- Korhonen, K., M. Kulmala, A. Laaksonen, Y. Vissanen, R. McGraw, and J.H. Seinfeld, Ternary nucleation of H<sub>2</sub>SO<sub>4</sub>, NH<sub>3</sub>, and H<sub>2</sub>O in the atmosphere, *J. Geophys. Res.*, 104, 26,349-26353, 1999.
- Kerminen, V.M., L. Pirjola, M. Kulmala, How significantly does coagulation limit atmospheric particle production?, *J. Geophys. Res.*, 106, 24,119-24,125, 2001.
- Kulmala, M., A. Laaksonen, and L. Pirjola, Parameterizations for sulfuric acid/water nucleation rates., *J. Geophys. Res.*, 103, 8301-8307, 1998.
- Ma, Y., R.J. Weber, Y.-N. Lee, A. Bandy, D. Thornton, A. Clarke, R. Blake, G. Sachse, H. Fuelberg, J.-H. Woo, D. Streets, G.R. Carmichael, and F.L. Eisele, The characteristics and influence of biomass burning aerosols on fine particle ionic composition measured in Asian Outflows during TRACE P, *J. Geophys. Res.*, *this issue*, 2002.
- Maloney, J. C., H.E. Fuelberg, M.A. Avery, J.H. Crawford, D.R. Blake, B.G. Heikes, G.W. Sachse, G.T. Sandholm, H. Singh, and R.W. Talbot, Chemical characteristics

- of air from different source regions during the second Pacific Exploratory Mission in the Tropics, *J. Geophys. Res.*, 106, 32609-32625, 2001.
- Marti, J.J., R.J. Weber, M.T. Saros, J.G. Vasilou, and P.H. McMurry, Technical Note: Modification of the TSI 3025 condensation particle counter for pulse height analysis, *Aerosol Sci. and Technol.*, 25, 214-218, 1996.
- McMurry, P.H., K.S. Woo, R.J. Weber, D.-R., Chen and D.Y.H. Pui, Size distributions of 3-10nm atmospheric particles: implication for nucleation mechanisms, *Phil. Trans. R. Soc. Lond. A*, 358, 2625-2642, 2000.
- Orsini, D., and R. Weber, A Particle-Into-Liquid Sampler (Pils) For Measurements Of Water Soluble Fine Aerosol Chemistry, *Atm. Environ.*, *under review*, 2002.
- Roedel, W., Measurement of sulfuric acid saturation vapor pressure; Implications for aerosol formation by heteromolecular nucleation, *J. Aerosol Sci.*, 10, 375-386, 1979
- Seinfeld, J.H., and S.N. Pandis, *Atmospheric Chemistry and Physics: From Air Pollution to Climate Change*, John Wiley and Sons, New York, 1998.
- Swietlicki, E., J. Zhou, D.S. Covert, K. Hameri, B. Busch, M. Vakeva, U., Dusek, O. H. Berg, A. Wiedensohler, P. Aalto, P., Makela, B. G. Marinsson, G. Papaspiropoulos, B. Mentes, G. Frank, F. and Stratmann., Hygroscopic properties of aerosol particles in the north-eastern Atlantic during ACE-2, *Tellus* 52B, 201-227, 2000
- Thornton, D. C., A. R. Bandy, F. H. Tu, B. W. Blomquist, G. M. Mitchell, W. Nadler, and D. H. Lenschow, Fast Airborne Sulfur Dioxide Measurements by Atmospheric Pressure Ionization Mass Spectrometry (APIMS), *J. Geophys. Res.*, submitted, 2002

- Weber, R.J., G. Chen, D.D. Davis, R.L. Mauldin, D.J. Tanner, F.L. Eisele, A.D. Clarke, D.C. Thornton, and A.R. Bandy, Measurements of enhanced H<sub>2</sub>SO<sub>4</sub> and 3-4 nm particles near a frontal cloud during ACE 1, *J. Geophys. Res.*, 106, 24,107-24,117, 2001a.
- Weber, R.J., J.J. Marti, P.H. McMurry, F.L. Eisele, D.J. Tanner, and A. Jefferson, Measurements of expected nucleation precursor species and 3 to 500 nm diameter particles at Mauna Loa Observatory, Hawaii, *J. Geophys. Res.*, 101, 14,767-14,775, 1995.
- Weber, R.J., J.J. Marti, P.H. McMurry, F.L. Eisele, D.J. Tanner, and A. Jefferson, Measured atmospheric new particle formation rates; Implications for nucleation mechanisms, *Chem. Eng. Commun.*, 151, 53-64, 1996.
- Weber, R.J., J.J. Marti, P.H. McMurry, F.L. Eisele, D.J. Tanner, A. Jefferson, Measurements of new particle formation and ultrafine particle growth rates at a clean continental site, *J. Geophys. Res.*, 102, 4,375-4,385, 1997.
- Weber, R.J., P.H. McMurry, L. Mauldin, D.J. Tanner, F.L. Eisele, F.J. Brechtel, S.M. Kreidenweis, G.L. Kok, R.D. Schillawski, D. Baumgardner, A study of new particle formation and growth involving biogenic and trace gas species measured during ACE 1, *J. Geophys. Res.*, 103, 16,385-16,396, 1998a.
- Weber, R.J., M. Stolsenburg, S. Pandis, and P.H. McMurry, Inversion of UCNC pulse height distributions to obtain ultrafine (~3 to 10nm) particle size distributions, *J. Aerosol. Sci.*, 29, 601-615, 1998b.

- Weber, R.J., A.D. Clarke, M. Litchy, J. Li, G. Kok, R.D. Schillawski, P.H. McMurry, Spurious aerosol measurements when sampling from aircraft in the vicinity of clouds, *J. Geophys. Res.*, 103, 28337-28346, 1998c.
- Weber, R.J., P.H. McMurry, R.L. Mauldin III, D.J. Tanner, F.L. Eisele, A.D. Clarke, V.N. Kapustin, New particle formation in the remote troposphere: A comparison of observations at various sites, *Geophys. Res. Lett.*, 26, 307-310, 1999.
- Weber, R.J., D. Orsini, Y. Daun, Y.N. Lee, P. J. Klotz, and F. Brechtel, A particle-into-liquid collector for rapid measurements of aerosol bulk chemical composition, *Aerosol Sci. Technol.*, 35, 718-727, 2001b.
- Wilemski, G., Composition of the critical nucleus in multicomponent vapor nucleation, *J. Chem. Phys.*, 80, 1370-1372, 1984.
- Williams, D.J., J.N. Carras, J.W. Milne and A.C. Heggie, The oxidation and long-range transport of sulphur dioxide in a remote region, *Atmos. Envir.*, 15, 2255-2262, 1981.
- Wilson, W.E., Sulfates in the atmosphere: A progress report on project MISTT, *Atmos. Envir.*, 12, 537-547, 1978.
- Woo, K. S., D.R. Chen, D.Y.H. Pui, P.H. McMurry, Measurement of Atlanta aerosol size distributions: Observations of ultrafine particle events, *Aerosol Sci. Technol.*, 34, 75-87, 2001.
- Yu, F., and R.P. Turco, From molecular clusters to nanoparticles: Role of ambient ionization in tropospheric aerosol formation, *J. Geophys. Res.*, 106, 4797-4814, 2001.

## **ACKNOWLEDGEMENTS**

The authors gratefully acknowledge the support of the National Atmospheric and Space Administration (NASA) under grant number NCC-1-411L. We also thank the many people from NASA Langley and the NASA Wallops Flight Facility for all their help during the experiment.

## Figure Captions

**Figure 1.** Flight paths near the Asian continental regions during TRACE-P and regions of high 3-4 nm particle concentration ( $>100 \text{ cm}^{-3}$ ).

**Figure 2.** Flight 19 path and 5-day back trajectories for Case 1, Sea of Japan. The region of plume interception is identified.

**Figure 3.** Time series plots for Case 1 (Sea of Japan, flight 19). (a) Altitude, (b) CO and  $\text{SO}_4^{2-}$ , (c)  $\text{SO}_2$  and  $\text{H}_2\text{SO}_4$ , (d) UCN and 3-4 nm particles, (e) aerosol surface area.

Shading identifies regions of 3-4-nm particle production.

**Figure 4.** Vertical profiles for the four soundings of Case 1, Sea of Japan, flight 19 shown in Figure 3. The mean and max/min are plotted as error bars.

**Figure 5.** Fine particle ( $D_p < 1.3 \mu\text{m}$ ) ionic mass in the Case Study 1, Sea of Japan plume. Mass concentrations are at  $20^\circ\text{C}$  and 1 atmosphere. An ion balance suggests most sulfate and nitrate is balanced by ammonium.

**Figure 6.** Flight 14 path and 5-day back trajectories for Case 2, Yellow Sea Plume. The region of plume interception is identified.

**Figure 7.** Time Series Plots for Case 2, Yellow Sea, flight 14. (a) Altitude, (b) CO and  $\text{SO}_4^{2-}$ , (c)  $\text{SO}_2$  and  $\text{H}_2\text{SO}_4$ , (d) total UCN and 3-4 nm particles, (e) Aerosol surface area. Shading identifies regions of 3-4-nm particle production.

**Figure 8.** Vertical profiles for the two soundings for the Yellow Sea plume of flight 14, Case 2 in Figure 7. (a) Relative humidity and temperature, (b) CO, (c) 3-4 nm particles, (d)  $\text{SO}_2$ , (e)  $\text{H}_2\text{SO}_4$ , (f) aerosol surface area.

**Figure 9.** Fine particle ionic composition for Yellow Sea plume, Case Study 2, Flight 14.

**Figure 10.** Comparison between measured and calculated  $\text{H}_2\text{SO}_4$  concentrations assuming steady state balance between OH- $\text{SO}_2$  production and loss onto preexisting particles. The data is for the regions near and within the plumes shown in Figures 3 and 7.

**Figure 11.** Surface area size distributions calculated from number distributions measured with an optical particle counter with inlet heated to  $40^\circ\text{C}$ . Particles are grown to ambient RH assuming uptake is by dust particles.

**Figure 12.** Comparison of the sulfuric acid concentrations and 3-4nm particles concentrations in the nucleation regions of the two plumes investigated and in a volcanic

plume. The data show that vapors other than  $\text{H}_2\text{SO}_4$  are also required for particle formation.

**Table 1.** Measured and Calculated Conditions of Nucleation and No Nucleation regions for Two Case Study Flights (F19 and F14) and Volcanic Plume (F17) During TRACE-P.

(A) Nucleation Above Plume- Case Study One - Sea of Japan - flight 19, N=16					
	Mean	Median	Max	Min	Standard Deviation
Altitude, km	1.57	1.41	2.11	1.39	0.27
Temperature, K	275	275.5	276	273	0.9
RH, %	33	32.5	44	18	7.7
CO, ppbv	203	208	257	153	29
SO <sub>2</sub> , pptv	1,679	1,752	2,884	588	652
OH, cm <sup>-3</sup> (x10 <sup>6</sup> )	4.60	4.39	6.85	3.05	1.12
H <sub>2</sub> SO <sub>4</sub> , cm <sup>-3</sup> (x10 <sup>7</sup> )	2.40	2.07	3.59	1.71	0.68
Relative Acidity (x10 <sup>-4</sup> )	8.20	7.75	12.50	5.79	0.19
3-4 nm particle, cm <sup>-3</sup>	175	139	431	82	95
UCN, cm <sup>-3</sup>	10,472	10,313	13,149	7,325	1,781
Surface Area, μm <sup>2</sup> cm <sup>-3</sup>	26	23	42	15	9.8
SO <sub>4</sub> <sup>2-</sup> , pptv	196	96	645	47	229
NH <sub>4</sub> <sup>+</sup> , pptv	677	402	1983	143	687
NH <sub>4</sub> <sup>+</sup> /SO <sub>4</sub> <sup>2-</sup> molar ratio	4.5	4.35	6	3.5	1
k' 1.5 nm, s <sup>-1</sup> (x10 <sup>-3</sup> )	1.2	0.82	0.24	4.0	1.1
k' H <sub>2</sub> SO <sub>4</sub> , s <sup>-1</sup> (x10 <sup>-3</sup> )	4.1	3.0	0.76	13	3.6
(B) No Nucleation Within Plume- Case Study One - Sea of Japan - flight 19, N=13					
Altitude, km	0.42	0.3	0.93	0.11	0.26
Temperature, K	282	282	285	277	2.6
RH, %	68	77	79	47	15
CO, ppbv	323	326	342	261	21
SO <sub>2</sub> , pptv	2,288	2,365	3,218	1,047	520
OH, cm <sup>-3</sup> (x10 <sup>6</sup> )	8.02	7.88	13.7	5.31	2.30
H <sub>2</sub> SO <sub>4</sub> , cm <sup>-3</sup> (x10 <sup>7</sup> )	1.97	1.72	3.10	1.38	0.57
Relative Acidity (x10 <sup>-4</sup> )	3.20	2.77	5.81	1.39	1.67
3-4 nm particle, cm <sup>-3</sup>	1	1	1.6	0.5	0.23
UCN, cm <sup>-3</sup>	5,080	4,984	6,665	4,022	691
Surface Area, μm <sup>2</sup> cm <sup>-3</sup>	171	182	217	111	34
SO <sub>4</sub> <sup>2-</sup> , pptv	2,618	2,739	3,133	1,565	525
NH <sub>4</sub> <sup>+</sup> , pptv	6,006	6,407	7,141	2,767	1,343
NH <sub>4</sub> <sup>+</sup> /SO <sub>4</sub> <sup>2-</sup> molar ratio	2.7	2.7	2.8	2.6	0.08
k' 1.5 nm, s <sup>-1</sup> (x10 <sup>-3</sup> )	3.0	3.1	1.4	4.8	0.79
k' H <sub>2</sub> SO <sub>4</sub> , s <sup>-1</sup> (x10 <sup>-3</sup> )	9.2	9.4	5.1	14.7	2.5

**Table 1.** Continued

(C) Nucleation - Case Study Two - Yellow Sea - flight 14, N=13					
	Mean	Median	Max	Min	Standard Deviation
Altitude, km	0.21	0.12	0.66	0.12	0.18
Temperature, K	284	284	286	282	1.2
RH, %	51	52.5	75	32	12.8
CO, ppbv	675	703	806	503	94
SO <sub>2</sub> , pptv	7,882	7,629	10,217	5,613	1,471
OH, cm <sup>-3</sup> (x10 <sup>6</sup> )	10.8	10.7	15.0	7.41	1.74
H <sub>2</sub> SO <sub>4</sub> , cm <sup>-3</sup> (x10 <sup>7</sup> )	5.95	6.28	8.83	2.78	2.22
Relative Acidity (x10 <sup>-4</sup> )	6.72	6.47	11.3	3.68	2.43
3-4 nm particle, cm <sup>-3</sup>	198	190	330	113	60
UCN, cm <sup>-3</sup>	11,896	12,285	14,440	8,211	2,108
Surface Area, μm <sup>2</sup> cm <sup>-3</sup>	744	735	1830	29	606
SO <sub>4</sub> <sup>2-</sup> , pptv	5,265	5,636	6,136	3,920	898
NH <sub>4</sub> <sup>+</sup> , pptv	17,435	19,262	20,133	3,354	19,262
NH <sub>4</sub> <sup>+</sup> /SO <sub>4</sub> <sup>2-</sup> molar ratio	3.75	3.73	3.8	3.7	0.05
k' 1.5nm, s <sup>-1</sup> (x10 <sup>-3</sup> )	3.87	4.12	2.5	9.4	3.2
k' H <sub>2</sub> SO <sub>4</sub> , s <sup>-1</sup> (x10 <sup>-3</sup> )	14	15	0.93	32	11
(D) No Nucleation - Case Study Two - Yellow Sea - flight 14, N=3					
Altitude, km	0.12	0.12	0.12	0.12	0
Temperature, K	282	282	282	282	0
RH, %	85	86	86	84	1.2
CO, ppbv	661	654	692	636	29
SO <sub>2</sub> , pptv	3,188	3,190	3,605	2,768	419
OH, cm <sup>-3</sup> (x10 <sup>6</sup> )	10.5	10.5	11.8	9.28	1.26
H <sub>2</sub> SO <sub>4</sub> , cm <sup>-3</sup> (x10 <sup>7</sup> )	1.56	1.53	1.77	1.37	2.01
Relative Acidity (x10 <sup>-4</sup> )	2.27	2.23	2.58	2.0	0.29
3-4 nm particle, cm <sup>-3</sup>	1	1	1	1	0
UCN, cm <sup>-3</sup>	5,821	5,813	6,025	5,626	200
Surface Area, μm <sup>2</sup> cm <sup>-3</sup>	1618	1553	1423	1879	235
SO <sub>4</sub> <sup>2-</sup> , pptv	4,040	4,040	4,040	4,040	0
NH <sub>4</sub> <sup>+</sup> , pptv	15,448	15,448	15,448	15,448	0
NH <sub>4</sub> <sup>+</sup> /SO <sub>4</sub> <sup>2-</sup> molar ratio	4.4	4.4	4.4	4.4	0
k' 1.5nm, s <sup>-1</sup> (x10 <sup>-3</sup> )	8.2	7.7	7.2	9.6	1.2
k' H <sub>2</sub> SO <sub>4</sub> , s <sup>-1</sup> (x10 <sup>-3</sup> )	25	23	21	32	5.7

**Table 1.** Continued

(F) Volcanic Plume - flight 17, N= 8					
	Mean	Median	Max	Min	Standard Deviation
Altitude, km	0.38	0.36	0.53	0.22	0.9
Temperature, K	286	286	288	285	1
RH, %	58	58	65	53	3.5
CO, ppbv	223	223	230	212	5.3
SO <sub>2</sub> , pptv	14,282	12,852	18,097	12,229	2,524
OH, cm <sup>-3</sup> (x10 <sup>6</sup> )	4.64	4.61	6.06	2.69	1.03
H <sub>2</sub> SO <sub>4</sub> , cm <sup>-3</sup> (x10 <sup>7</sup> )	17.8	16.6	21.5	14.6	2.82
Relative Acidity (x10 <sup>-4</sup> )	16.1	14.9	22.4	12.7	3.44
3-4 nm particle, cm <sup>-3</sup>	3.7	2.6	6.8	1.79	1.98
UCN, cm <sup>-3</sup>	8,960	9,108	9,859	7,263	778
SO <sub>4</sub> <sup>2-</sup> , pptv	3,317	3,222	4,126	3,084	340
NH <sub>4</sub> <sup>+</sup> , pptv	2,731	2,772	2,875	2,342	175

N: Number of data points, except for surface area and scavenging time, which have fewer points.

k' is the rate constant for loss of 1.5 nm particles or H<sub>2</sub>SO<sub>4</sub> onto the preexisting aerosol determined from the method of *Fuchs-Sutugin* [1970].

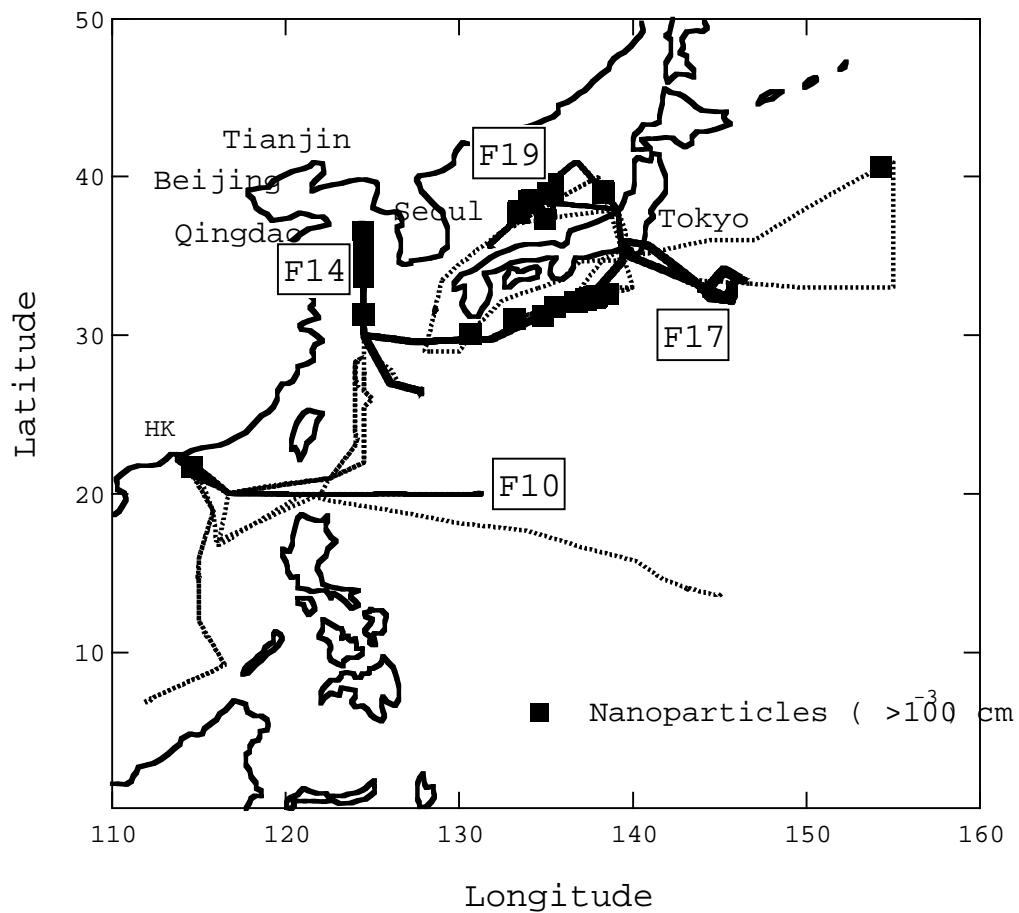
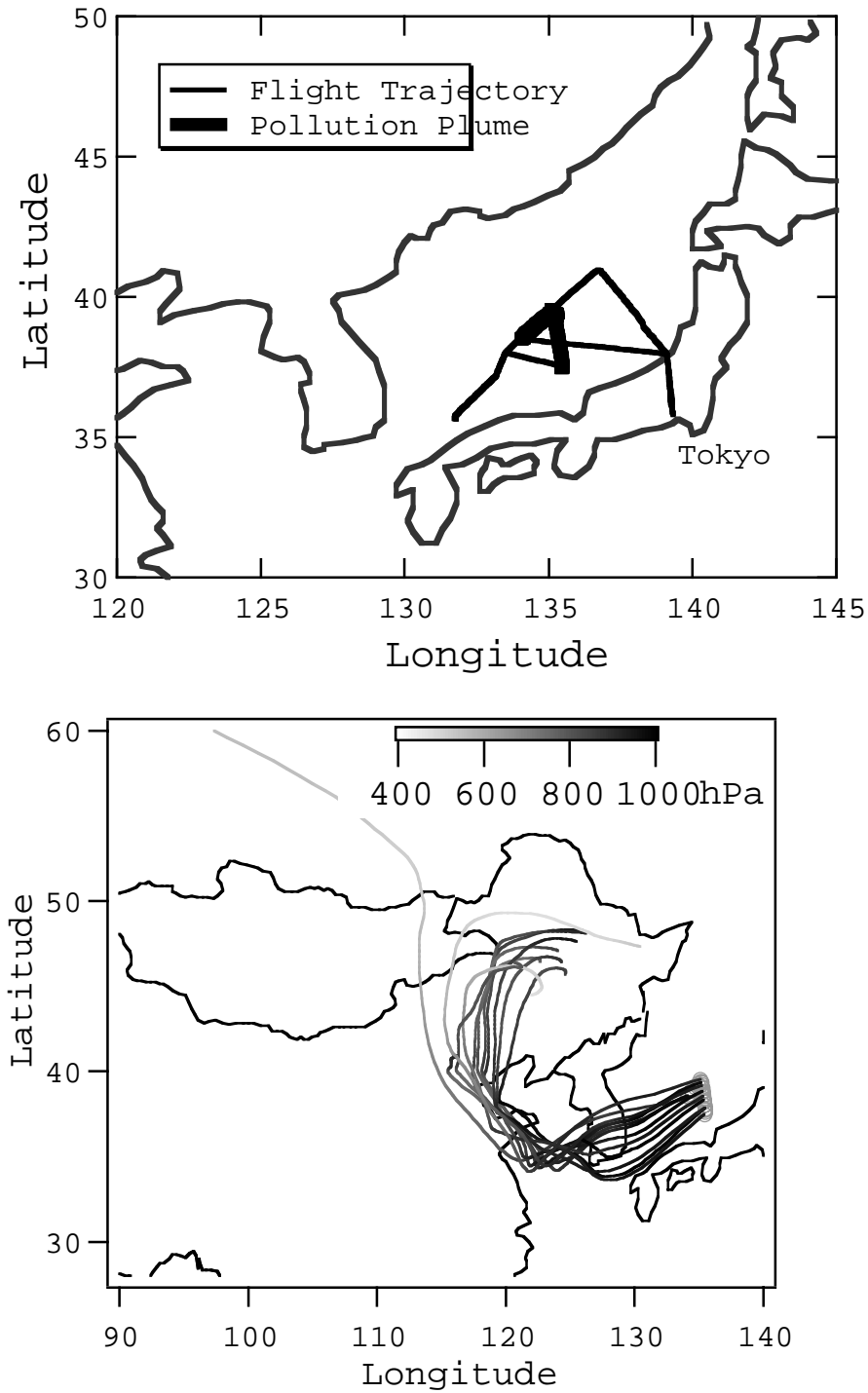
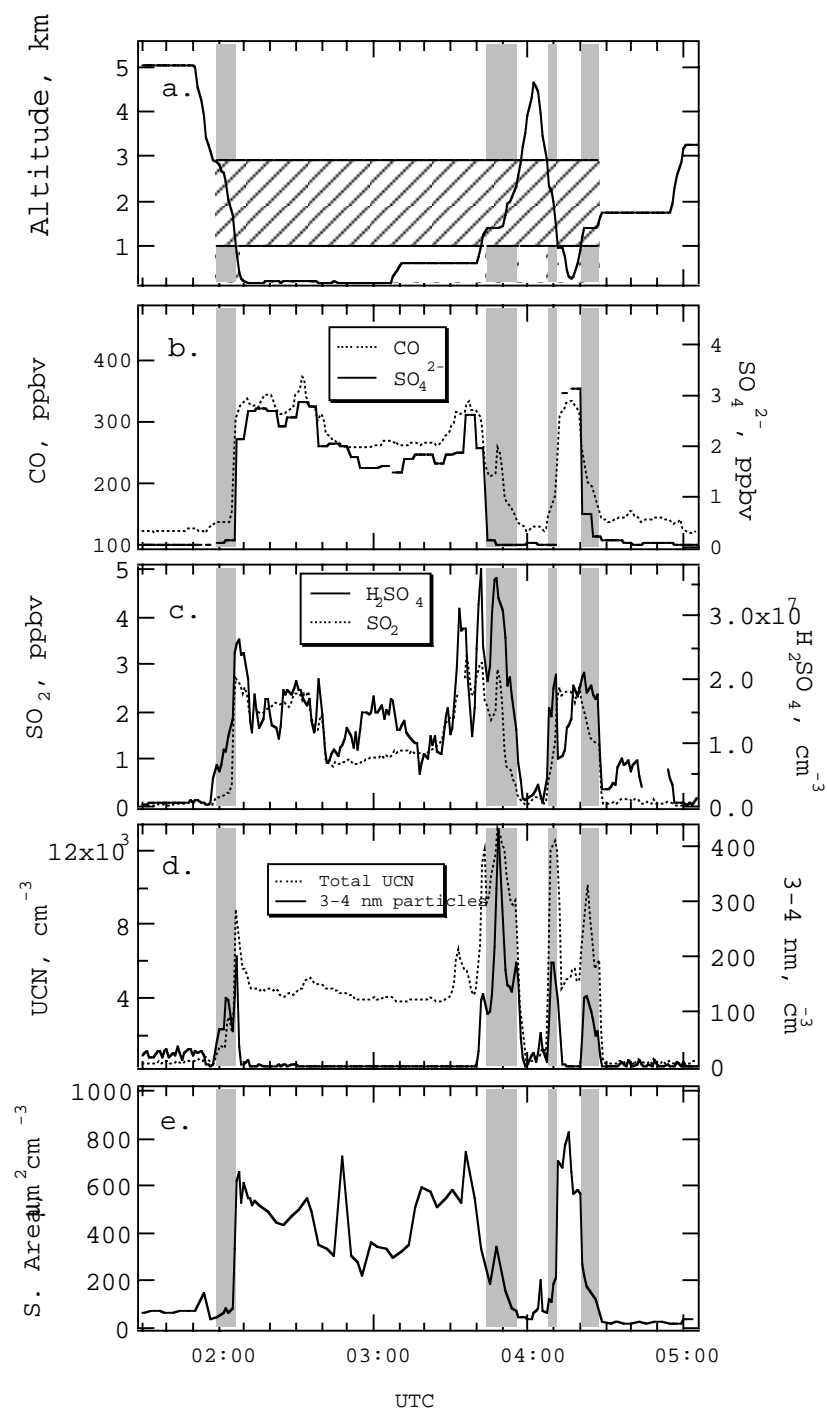


Figure 1 Flight paths near the Asian continental regions during 3-4 nm particle concentration. ( $>10^3 \text{ cm}^{-3}$ )



**Figure 2.** Flight path and 5-day back trajectories for Case 1 (Sea of Japan). The location of the plume is identified.



**Figure 3** Time series plots for Case 1 (Sea of Japan, flight 19). (a) Altitude, (b) CO and  $\text{SO}_4^{2-}$ , (c)  $\text{SO}_2$  and  $\text{H}_2\text{SO}_4$ , (d) total UCN and 3-4 nm particles, (e) aerosol surface area. Shading identifies regions of 3-4 nm particle production.

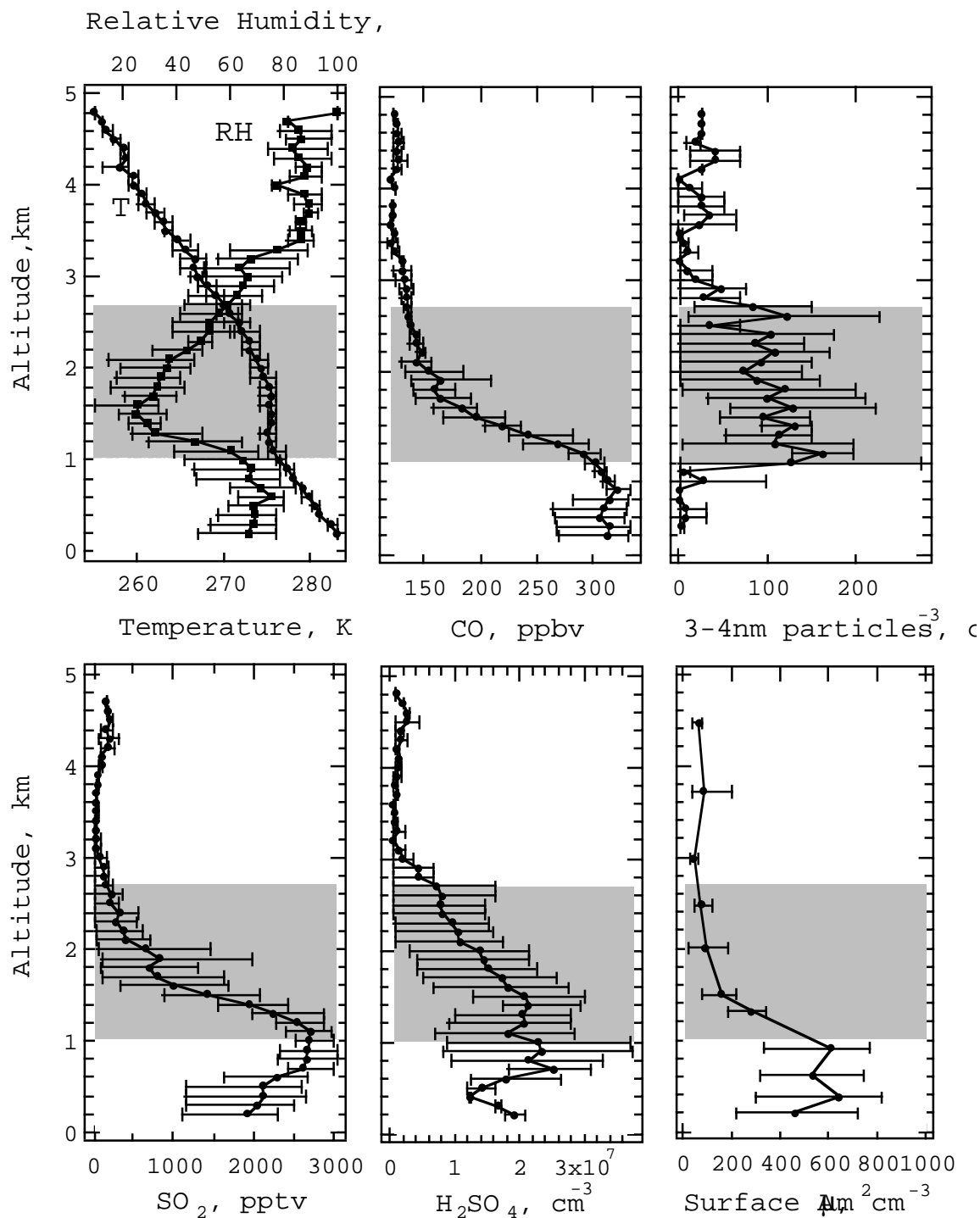


**Figure 4** Vertical profiles for the four soundings of Case 1 (Sea of Japan, flight 19) shown in Figure 3. The mean and max/min are plotted as error bars.

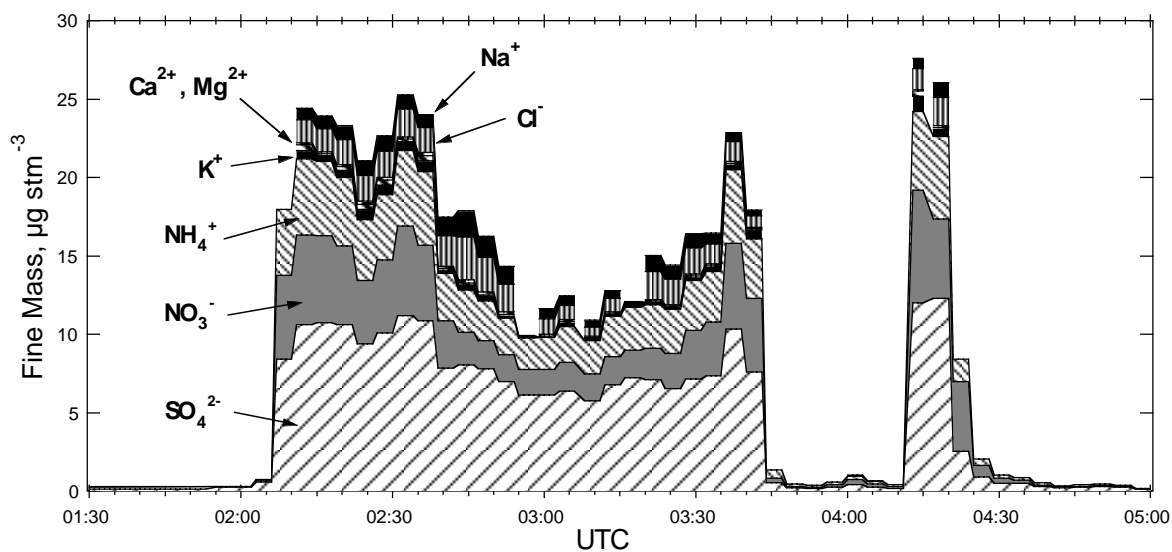
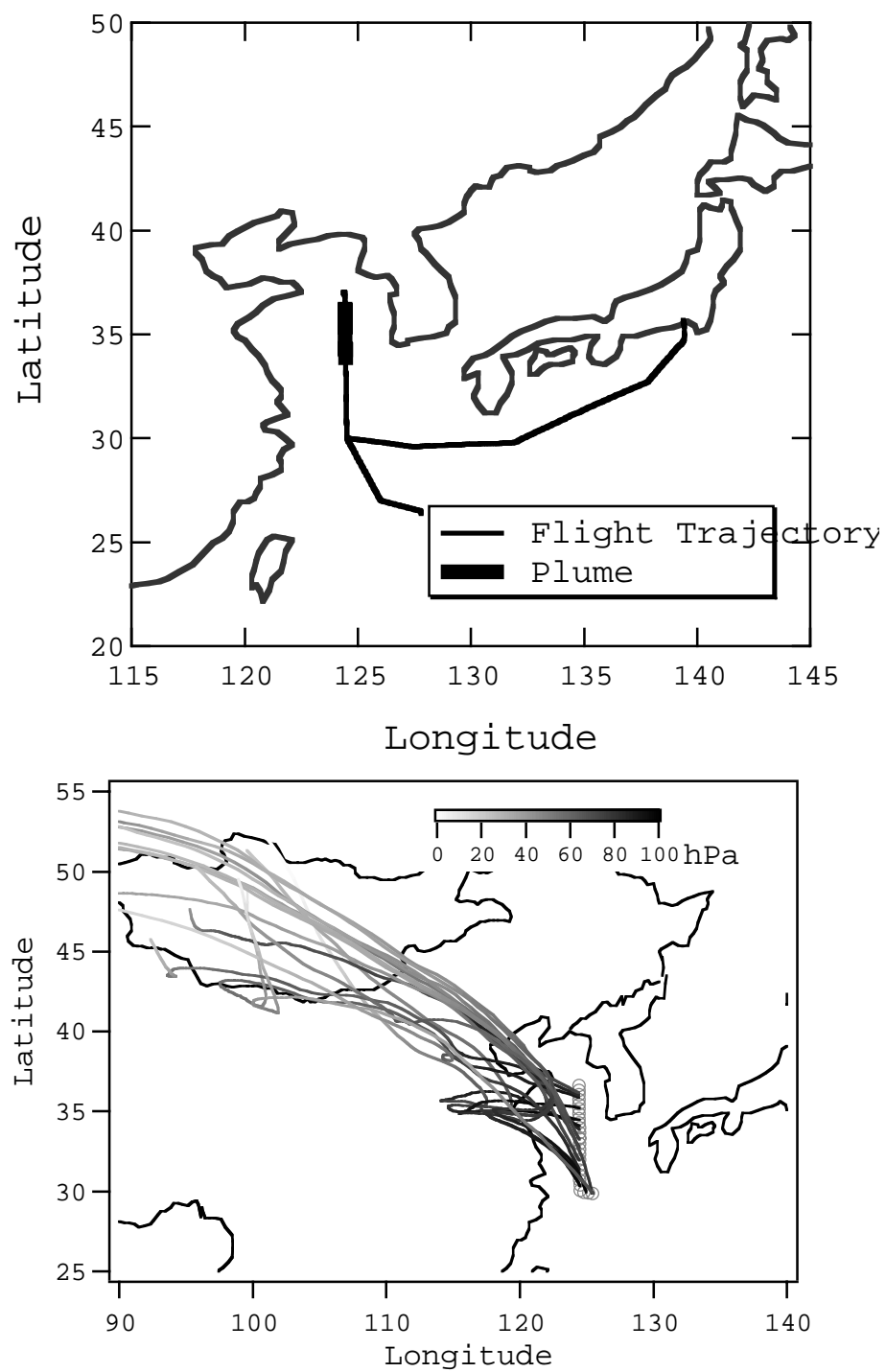
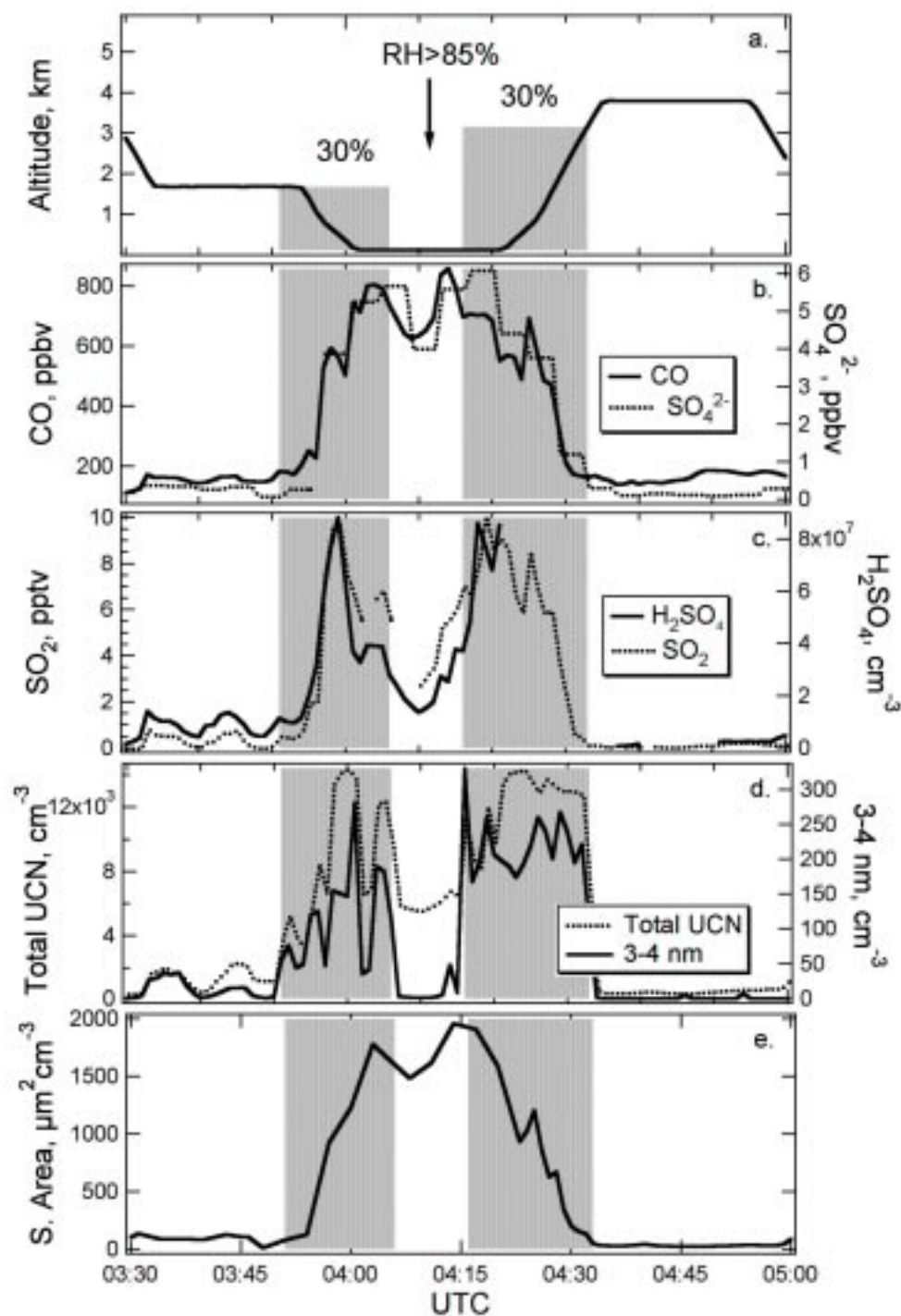


Figure 5, Fine particle ( $D_p < 1.3 \mu\text{m}$ ) ionic mass in the Case Study 1, Sea of Japan plume. Mass concentrations are at 20°C and 1 atmosphere. An ion balance suggests most sulfate and nitrate is balanced by ammonium.



**Figure 6** Flight path and 5-day back trajectories for Case 2 (Yellow Sea, flight 14). The location of pollution plume is also identified.



**Figure 7** Time Series Plots for Case 2, Yellow Sea, flight 14. (a) Altitude, (b) CO and  $\text{SO}_4^{2-}$ , (c)  $\text{SO}_2$  and  $\text{H}_2\text{SO}_4$ , (d) UCN and 3-4 nm particles, (e) Aerosol surface area.

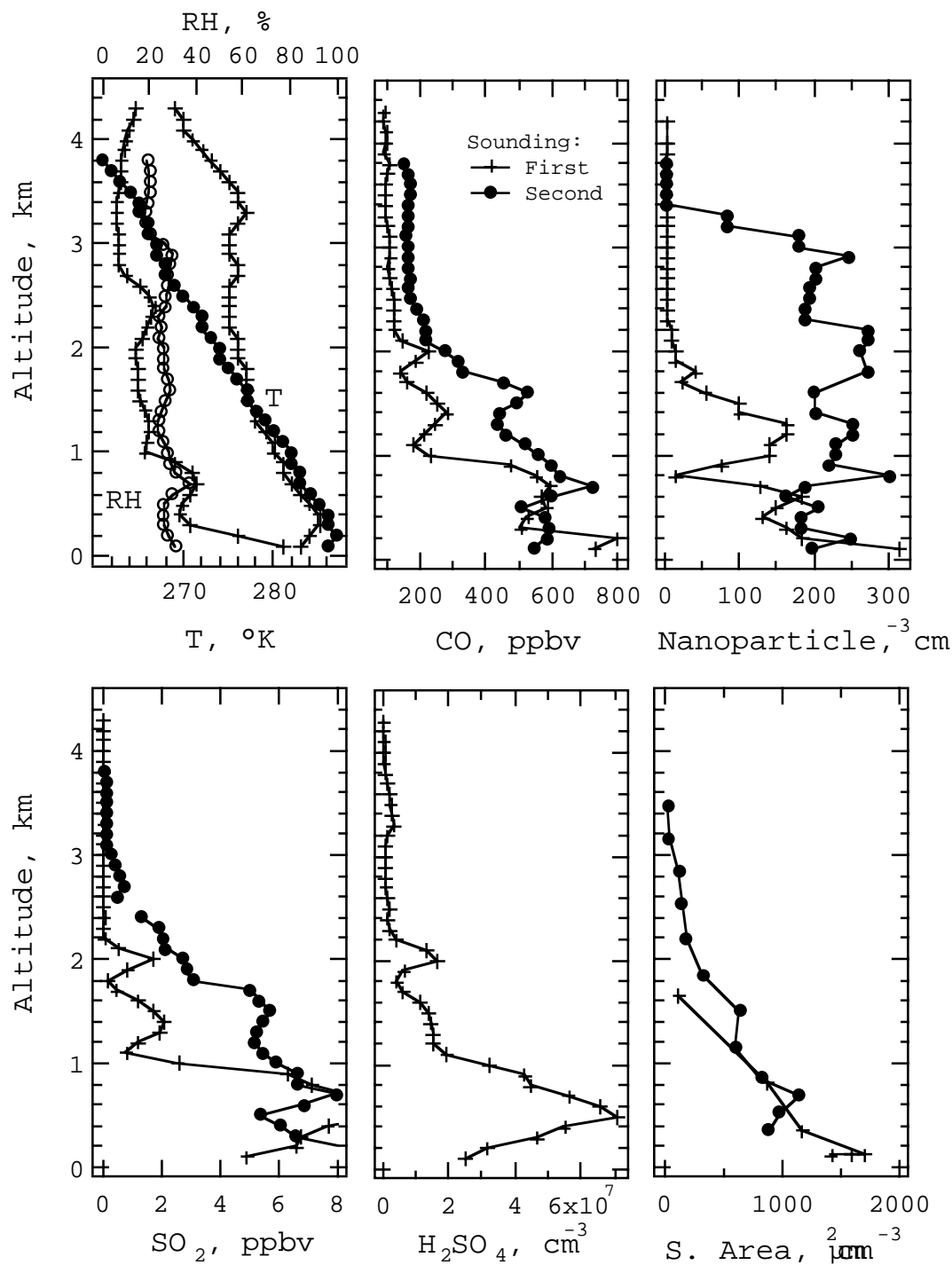


**Figure 8** Vertical profiles for the soundings of Case 2, the Yellow Sea plume of flight 14 in Figure 7. (a) Relative humidity and temperature, (b) CO, (c) 3-4 nm particles, (d)  $\text{SO}_2$ , (e)  $\text{H}_2\text{SO}_4$ , (f) aerosol surface area.

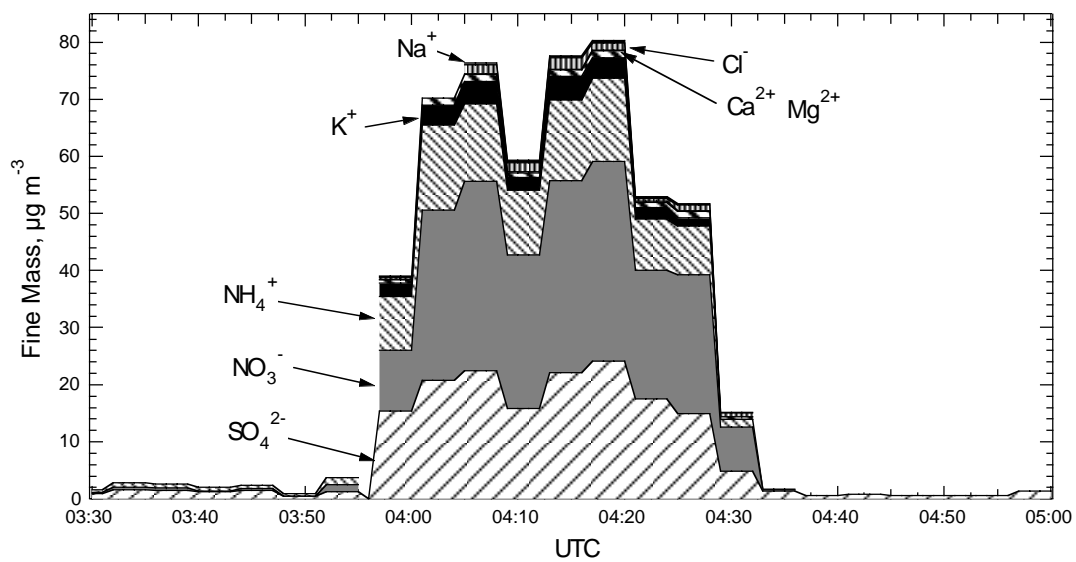
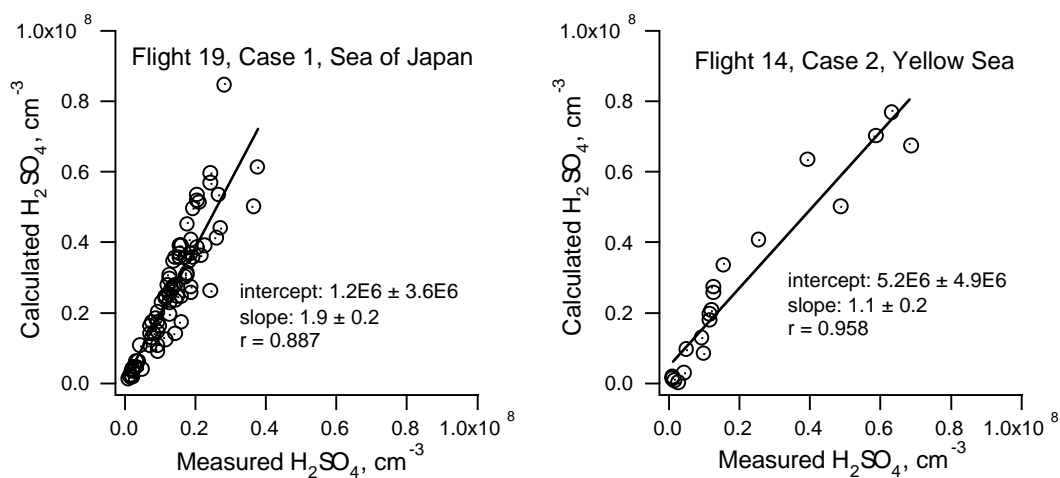
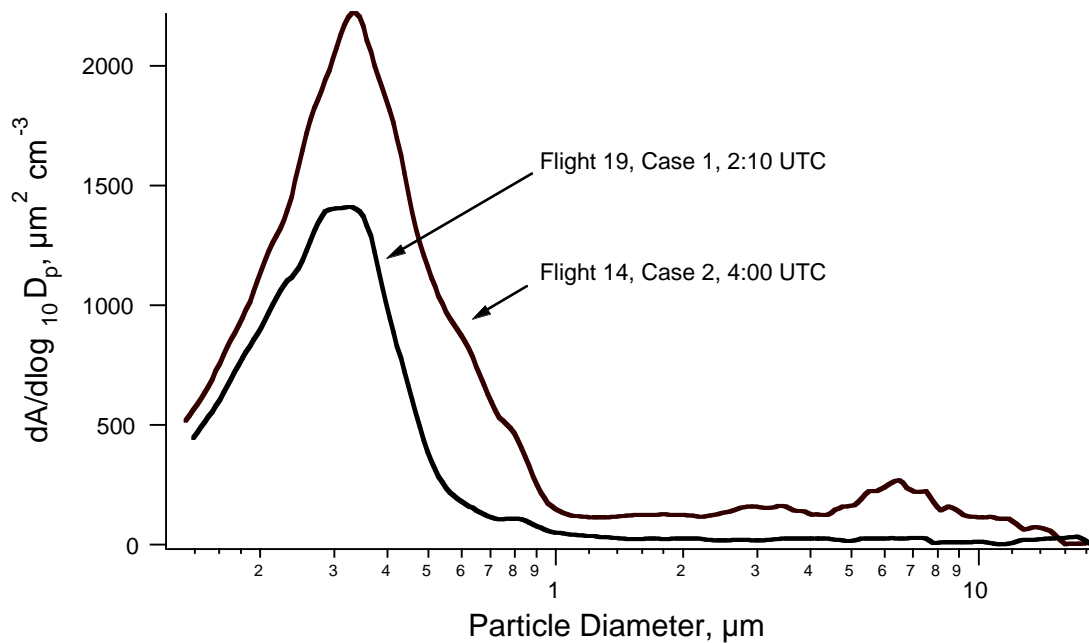


Figure 9 Fine particle ionic composition for Yellow Sea plume, Case Study 2, Flight 14.



**Figure 10.** Comparison between measured and calculated  $\text{H}_2\text{SO}_4$  concentrations assuming steady state balance between  $\text{OH-SO}_2$  production and loss onto preexisting particles. The data is for the regions near and within the plumes shown in Figures 3 and 7.



**Figure 11.** Surface area size distributions calculated from number distributions measured with an optical particle counter with inlet heated to 40°C. Particles are grown to ambient RH assuming uptake is by dust particles.

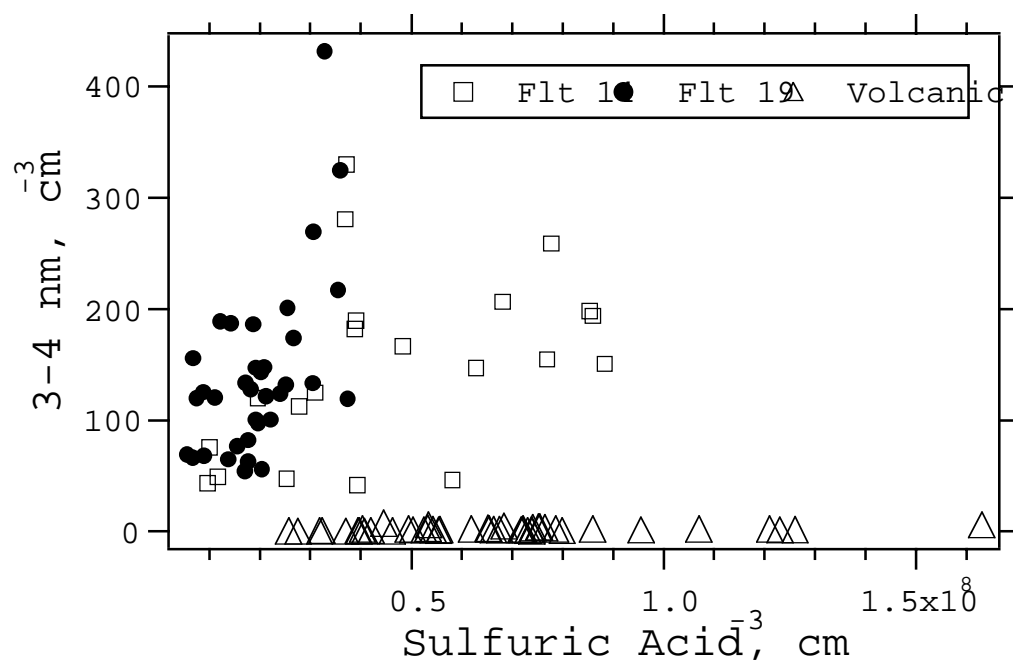


Figure 12. Comparison of the sulfuric acid concentrations and 3-4nm particles concentrations in the nucleation regions of the two plumes investigated and in a volcanic plume. The data show that vapors other than H<sub>2</sub>SO<sub>4</sub> are also required for particle formation.